Eur. J. Biochem. **268,** 4950–4960 (2001) © FEBS 2001

Application of radiolabeled tracers to biocatalytic flux analysis

Kurt S. Yanagimachi[1], Daniel E. Stafford[1], Annette F. Dexter[2], Anthony J. Sinskey[2], Stephen Drew[3] and Gregory Stephanopoulos[1]

[1]*Department of Chemical Engineering and* [2]*Department of Biology, Massachusetts Institute of Technology, Cambridge, USA;* [3]*Department of Bioprocess Research and Development, Merck Research Laboratories, Merck & Co., Rahway, NJ, USA*

Radiolabeled tracers can provide valuable information about the structure of and flux distributions in biocatalytic reaction networks. This method derives from prior studies of glucose metabolism in mammalian systems and is implemented by pulsing a culture with a radiolabeled metabolite that can be transported into the cells and subsequently measuring the radioactivity of all network metabolites following separation by liquid chromatography. Intracellular fluxes can be directly determined from the transient radioactivity count data by tracking the depletion of the radiolabeled metabolite and/or the accompanying accumulation of any products formed. This technique differs from previous methods in that it is applied within a systems approach to the problem of flux determination. It has been used for the investigation of the indene bioconversion network expressed in *Rhodococcus* sp. KY1. Flux estimates obtained by radioactive tracers were confirmed by macroscopic metabolite balancing and showed that indene oxidation in steady state chemostat cultures proceeds primarily through a monooxygenase activity forming (1*S*,2*R*)-indan oxide, with no dehydrogenation of *trans*-(1*R*,2*R*)-indandiol. These results confirmed the significance of indan oxide formation and identified the hydrolysis of indan oxide as a key step in maximizing the production of (2*R*)-indandiol, a chiral precursor of the HIV protease inhibitor, Crixivan®.

Keywords: metabolic flux; radiolabeled tracers; indene; *Rhodococcus*; metabolic engineering.

Rational improvement of cellular properties through metabolic engineering requires detailed knowledge of cell physiology, in particular as expressed by fluxes and flux distributions through key intracellular pathways. Metabolic flux analysis provides a framework for determining pathway fluxes from the stoichiometry of the pathway reactions in combination with extracellular metabolite measurements [1–3]. Rates of metabolite consumption and production, conveniently measured in chemostat experiments, usually provide the necessary information to calculate the fluxes. Batch and fed-batch systems have also been used occasionally. This framework has been applied to many biological systems, such as lysine production in *Corynebacterium glutamicum* [4,5], and central carbon metabolism in *Escherichia coli* [6–9], yeast [10,11], hybridoma cells [12–14], and organ tissue [15], among others.

Metabolic flux analysis can be further enhanced with the inclusion of additional measurement techniques providing more detailed flux information than that embedded in typical extracellular metabolite data. Such information is particularly important for the study of underdetermined systems, which occur when the number of unknown fluxes exceeds the number of available flux measurements and metabolite balances [2]. This is usually the case with highly interconnected networks or networks comprising metabolic cycles [16]. The basis of such measurement methods is the use of isotope labels. For example, ^{13}C-labeling can yield flux information from carbon enrichment measurements obtained by NMR spectroscopy as has been amply demonstrated in bacterial cultures [17–20], mammalian cell cultures [21–24], organ tissue [25–29], and erythrocytes [30,31]. Results from ^{13}C-tracer experiments have also been used to confirm flux estimates obtained through material balances [13,32]. Additionally, the quantitative use of GC-MS for flux determination from the measurement of mass isotopomers of various metabolites holds great promise for more detailed flux and metabolic network analysis [33].

For bioreaction networks in which there is no alteration of the metabolite carbon structure, direct determination of a metabolic flux can be accomplished using a radioactive isotope tracer. We describe this method here. The general approach is similar to the bolus-injection (impulse) technique developed for the study of glucose metabolism in mammalian systems [34–36]. In these studies, labeled glucose was injected intravenously in rats, dogs, humans, and cows, and radioactive kinetic data was used to calculate the rate of plasma glucose absorption. Networks of bioconversion reactions can be similarly analyzed. By pulsing a radiolabeled substrate and/or pathway intermediate(s) into a sample of microbial culture, uptake and intracellular fluxes can be determined from transient intensity measurements of the radiolabeled substrate and its products. As radioactive compounds can be measured with high sensitivity relative to stable isotope tracers, only trace amounts are required to probe cell physiology. Thus, the perturbation of the cellular state under analysis is minimized. These measurements are extremely valuable in a systems approach to bioreaction network analysis that studies multiple reactions simultaneously within a single mathematical framework, in contrast with previous work that generally focused on a single reaction. The tracer measurements can be used for: (a) confirming flux estimates obtained from extracellular metabolite measurements; (b) allowing full flux determination in those cases

Correspondence to G. Stephanopoulos, Massachusetts Institute of Technology, Room 56-469C, 77 Massachusetts Avenue, Cambridge, MA 02139, USA. Fax: + 1 617 253 3122, Tel.: + 1 617 253 4583, E-mail: gregstep@mit.edu

(Received 5 June 2001, revised 25 July 2001, accepted 30 July 2001)

that cannot be resolved by extracellular measurements alone; and (c) validating the structure of a bioconversion pathway.

In this study, radiolabeled tracers were applied to a model bioconversion network of enzymatic reactions expressed in *Rhodococcus*. Several strains (such as *Rhodococcus* sp. I24, see Fig. 1) were isolated that contain the enzymatic machinery for converting indene to indandiol (an intermediate in the production of (−)-*cis*-(1*S*,2*R*)-1-aminoindan-2-ol [(−)-CAI]), a key precursor in the synthesis of Merck's HIV protease inhibitor, Crixivan® [37,38]. In general, biocatalysis is advantageous for the synthesis of chiral compounds over traditional synthetic chemistry methods because the latter often yields racemic mixtures that require costly separations of the enantiomeric components. Extensive chemostat studies carried out with I24 yielded a new strain, *Rhodococcus* sp. KY1, with drastically improved bioconversion characteristics by virtue of oxidizing indene to fewer undesired products relative to I24 as elucidated from [^{14}C]indene tracer analysis (Fig. 1) (D. E. Stafford, K. S. Yamaguchi, P. A. Lessard, S. K. Rijhwani, A. J. Sinskey & G. Stephanopoulos, unpublished results). This network comprises oxygenase enzymes that convert indene to indan oxide and indandiol through monooxygenase and dioxygenase enzyme activities, respectively. The *cis*-indandiols are further converted to 1-keto-2-hydroxy-indan through dehydrogenase enzymes. Material balancing alone is not sufficient to determine all of the intracellular fluxes in the KY1 network. This requires additional flux information to be gathered using radiolabeled tracers for the complete elucidation of the network.

We present here a method for flux determination using ^{14}C-tracers, along with results demonstrating the relative importance of the KY1 enzymes in the formation of (2*R*)-indandiol products. Such information is useful in defining targets for genetic modification to engineer strains with improved biosynthesis of (2*R*)-indandiol. In its present form, the KY1 bioconversion network contains an oxygenase reaction that converts indene to the undesired *cis*-(1*R*,2*S*)-indandiol enantiomer and a dehydrogenase reaction further converts the desired *cis*-(1*S*,2*R*)-indandiol product to racemic 1-keto-2-hydroxy-indan byproduct. Undesired pathways with significant relative fluxes should be the primary targets for genetic knockouts as they will have the greatest impact on increasing product yield.

MATERIALS AND METHODS

Microorganisms and preparation of cell lysates

Rhodococcus sp. KY1 was isolated during a continuous fermentation of *Rhodococcus* sp. I24 (D. E. Stafford, K. S. Yamaguchi, P. A. Lessard, S. K. Rijhwani, A. J. Sinskey & G. Stephanopoulos, unpublished results). Stock cultures of KY1 were stored at −80 °C in Luria–Bertani medium supplemented with 25% glycerol. *Rhodococcus* sp. B264-1 was isolated by Merck scientists from soil contaminated with hydrocarbons [38]. *Rhodococcus* sp. SQ1(pR4) was obtained by transforming SQ1 with I24 cosmid DNA containing the *nidABCD* genes [39]. Working colonies of B264-1 and SQ1(pR4) were grown and maintained on Luria–Bertani plates streaked from frozen stocks stored at −80 °C.

Cell lysates were prepared by collecting cells from the chemostat outlet and centrifuging at 27 000 ***g***. The supernatant was removed and the cells were washed in lysis buffer at pH 7.6 containing 100 mM Hepes, 10% glycerol, 0.2 mM 2-mercaptoethanol, and two tablets per 50 mL of protease inhibitor cocktail (Complete, EDTA-free, Boehringer Mannheim, GmbH, Germany). The cells were centrifuged and resuspended in lysis buffer. The cell suspensions were then passed through a prechilled French press at 16 000 p.s.i. three times.

Synthesis of [^{14}C]indene and [^{14}C](1S,2R)-indan oxide

The synthesis of [^{14}C]indene was carried out with an overall 58% radiochemical yield from [^{14}C]benzene (**1**) as shown in Fig. 2. The first step utilized a one-pot Friedel–Crafts acylation/cyclization to form 1-indanone (**3**) [40]. The *enol*-triflate (**4**) was then formed, which was easily reduced with Pd(0)/triethylsilane to produce [^{14}C]indene [41,42]. The volatile nature of indene necessitated careful handling and isolation of this tracer. The high solubility of indene, as well as intermediates **3** and **4**, in pentane allowed for solution handling and solvent removal with minimal loss of product. The crude [^{14}C]indene was purified by prep HPLC (Zorbax SB-C18, 26 × 250 mm, acetonitrile/water, 40 : 60–60 : 40) and isolated from the column fractions via liquid/liquid extraction with pentane followed by a switch of solvent to ethanol. The tracer was thus supplied as

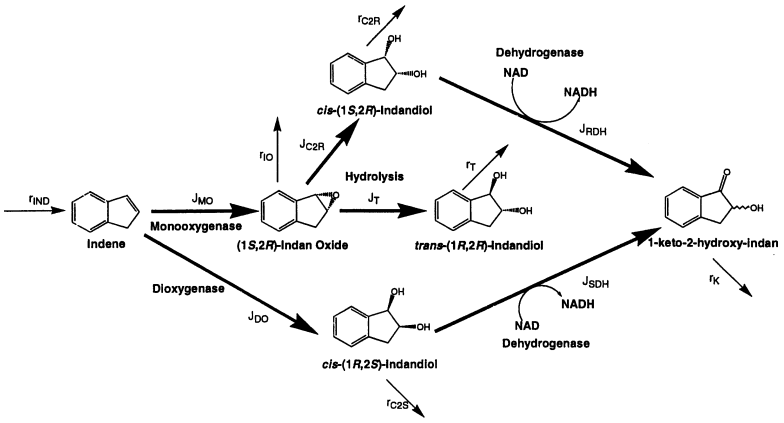

Fig. 1. Pathways of indene bioconversion in *Rhodococcus* sp. KY1, a mutant of I24 selected during chemostat fermentation. J_i are the pathway fluxes calculated through material balancing (except for J_{RDH}) and r_i are the production/uptake rates determined from steady state chemostat measurements. $r_i = D{\cdot}c_i$ where D is the chemostat dilution rate (h^{-1}) and c_i is the steady state extracellular metabolite concentration ($mg{\cdot}L^{-1}$). I, indene; IO, indan oxide; T, *trans*-(1*R*,2*R*)-indandiol; C2R, *cis*-(1*S*,2*R*)-indandiol; C2S, *cis*-(1*R*,2*S*)-indandiol; K, 1-keto-2-hydroxy-indan.

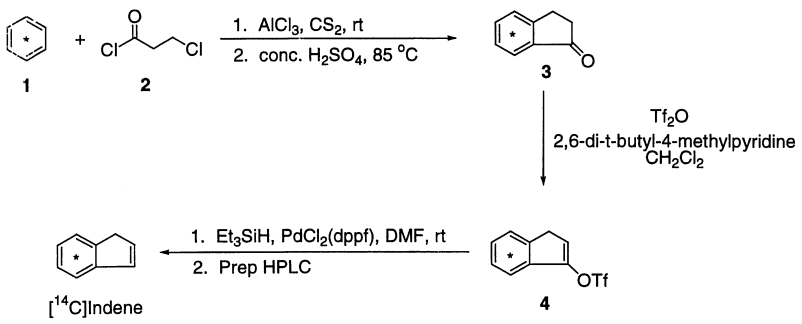

Fig. 2. [^{14}C]Indene synthesis scheme.

an ethanol solution (29 mCi, 425 μCi·mg^{-1}, in 7 mL of ethanol, > 99.6% radiochemical purity by HPLC).

[^{14}C](1*S*,2*R*)-indan oxide was prepared by the enantioselective epoxidation of [^{14}C]indene via the Jacobsen method (Fig. 3) [43]. The selective epoxidation yielded material of ≈ 80% enantiomeric excess that was upgraded to 98% enantiomeric excess via chiral prep-HPLC purification following filtration on crude silica (Chiralcel OB, 20 × 250 mm, hexane/ethanol, 95 : 5). The elution buffer was run isocratically at 0.8 mL·min^{-1}, and the (1*S*,2*R*)-indan oxide fraction eluted at 11.0 min. The tracer was supplied as a heptane solution (0.855 mCi, 374 μCi·mL^{-1}, in 4.64 mL of heptane).

Biosynthesis of [^{14}C]indandiols

Indandiol enantiomers were synthesized from oxidation of [^{14}C]indene with different *Rhodococcus* strains. KY1 was used to synthesize *trans*-(1*R*,2*R*)-indandiol, B264-1 was used to synthesize *cis*-(1*S*,2*R*)-indandiol, and SQ1(pR4) was used to synthesize *cis*-(1*R*,2*S*)-indandiol. One-milliliter precultures were prepared from the working cultures of each strain, and were used to inoculate two 250-mL shake flasks for each strain containing 25 mL of complex medium [38]. The cultures were grown overnight, and 0.5 mCi of [^{14}C]indene was then added to each flask. The KY1 and SQ1(pR4) cultures were grown with [^{14}C]indene for 24 h and the B264-1 cultures were grown with [^{14}C]indene for 48 h. The two flasks of each culture were combined in a single flask. Fifty milliliters of ethyl acetate and approximately 2 g of NaCl was added to each culture flask, and each mixture was agitated to extract the metabolites into the ethyl acetate layer. The mixture was transferred to 50-mL centrifuge tubes and centrifuged at 15 000 ***g*** to separate the two liquid phases. The ethyl acetate soluble fraction was reduced to dryness by rotary evaporation and the residue was redissolved in 500 μL of isopropanol. The indandiols in the mixture were then purified by semipreparative HPLC with a Zorbax Rx-C8 column (acetonitrile/water, 85 : 15–60 : 40 at 20 min to 0 : 100 at 30 min). The HPLC fractions containing the appropriate indandiols were reduced to dryness under a nitrogen sweep and redissolved in water. The activities of each fraction were as follows: 167 μCi of [^{14}C]*cis*-(1*R*,2*S*)-indandiol in 1 mL of water, 82 μCi of [^{14}C]*cis*-(1*S*,2*R*)-indandiol in 1 mL of water, and 40 μCi of [^{14}C]*trans*-(1*R*,2*R*)-indandiol in 2 mL of water.

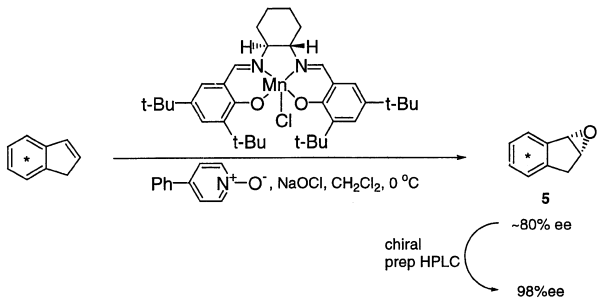

Fig. 3. [^{14}C](1*S*,2*R*)-Indan oxide synthesis scheme.

Chemostat system

KY1 was grown in a 1.0-L continuous flow bioreactor (chemostat) with indene delivered continuously through the gas phase (D. E. Stafford, K. S. Yamaguchi, P. A. Lessard, S. K. Rijhwani, A. J. Sinskey & G. Stephanopoulos, unpublished results). The dilution rate (based on the medium feed flow rate) and indene air feed concentration were maintained at constant levels until the culture reached steady state. The steady state was defined as being when constant biomass and indene metabolite concentrations (within 5% relative error) were achieved for at least four residence times.

Reverse-phase HPLC assay for ^{14}C-labeled metabolite experiments

Reverse-phase HPLC was used to separate the indene-derived metabolites, obtain radioactive counts of labeled metabolites and measure the metabolite concentrations during the ^{14}C-transient experiments. Two-hundred-microliter samples from the shake flask were placed into 200 μL of a 1 : 1 (v/v) mixture of acetonitrile and isopropyl alcohol. The microtubes containing this mixture were centrifuged to pellet the cells. The supernatant was filtered using 0.2 μm poly(vinylidene difluoride) 13 mm syringe filters (Alltech, Deerfield, IL, USA) into an HPLC sample vial. Ten microliters of the filtrate was injected into an HPLC system (Hewlett Packard Series 1050, San Fernando, CA, USA) equipped with a Zorbax RX-C8 column (4.6 mm × 25 cm) (Hewlett Packard). The HPLC protocol was followed as described previously [37]. The chirality of the *cis*-indandiol was determined using a normal phase HPLC Chiralpak AD column (Chiral Technologies, Inc., Exton, PA, USA) as described previously [38]. The UV detector was used to quantify the concentrations of each unlabeled metabolite pool for each time point in the ^{14}C-transient experiments.

A flow scintillation analyzer (Radiomatic 150TR, Packard Instrument Co., Meriden, CT, USA) was connected downstream of the UV detector for quantification of the ^{14}C

radioactive counts. For the 1 mL·min^{-1} flow rate through the HPLC, 3 mL·min^{-1} of liquid scintillation cocktail (Ultima-Flo M, Packard Instrument Co.) was mixed in the analyzer. The peaks for each radioactive metabolite detected in the chromatogram were integrated, and the total accumulated counts were reported.

Indan oxide hydrolysis experiments

One milliliter of KY1 cell lysate was placed in a 5-mL screw-cap vial and 4.3 μL of the [^{14}C](1*S*,2*R*)-indan oxide stock was added. The lysate was agitated with a magnetic stirrer and maintained at 4 °C. Samples were taken for 12 h after [^{14}C]indan oxide addition.

^{14}C-Tracer experiments for flux determination

Five separate 125 mL screw-cap shake flasks were prepared for measuring the transient profiles of five different ^{14}C-compounds: indene, (1*S*,2*R*)-indan oxide, *trans*-(1*R*,2*R*)-indandiol, *cis*-(1*R*,2*S*)-indandiol, and *cis*-(1*S*,2*R*)-indandiol. Fifteen milliliters of culture from the chemostat at steady state was placed into each shake flask. The ^{14}C-metabolites were immediately added to the flasks in the following amounts: 50 μL of aqueous ethanol containing 425 μCi·mL^{-1} [^{14}C]indene, 50 μL of heptane containing 374 μCi·mL^{-1} of [^{14}C](1*S*,2*R*)-indan oxide, 50 μL of water containing 167 μCi·mL^{-1} [^{14}C]*cis*-(1*R*,2*S*)-indandiol, 50 μL of water containing 82 μCi·mL^{-1} [^{14}C]*cis*-(1*S*,2*R*)-indandiol, and 50 μL of water containing 40 μCi·mL^{-1} [^{14}C]*trans*-(1*R*,2*R*)-indandiol. The flasks were maintained at 30 °C in a shaker at 300 r.p.m. Samples were taken periodically for 2 h for radioactive count and concentration measurements.

Intracellular concentration measurement

The protocol for determining cell volume was adapted from a method described previously [44]. This procedure was verified by measuring the cell volume of *Corynebacterium glutamicum*. Clement *et al*. [45] reported a cell volume of 1.76 ± 0.20 μL per mg per dry cell weight while a cell volume of 2.22 ± 0.03 μL per mg per dry cell weight was measured using the procedure from [44]. The protocol for isolating the intracellular metabolites was adapted from a method described previously [46]. The intracellular amounts were measured using reverse-phase HPLC.

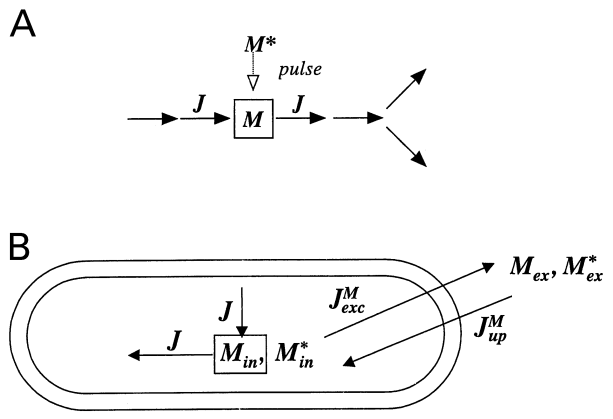

Fig. 4. Schematic pathway for direct flux determination (A) and for flux determination including uptake and excretion fluxes following tracer pulse (B).

Model of tracer labeling dynamics

The approach followed here to determine intracellular pathway fluxes is similar to that applied previously in the study of human metabolism *in vivo* [47]. It is noted that an important distinction of the indene bioreaction system (Fig. 1) is that it is decoupled from primary carbon-energy metabolism in terms of carbon flux by supplying a separate glucose feed as a carbon source, as indene is not used by these *Rhodococcus* isolates for this purpose; additionally, indene cannot be synthesized from glucose as indicated by indene metabolite balancing. Indene bioconversion can thus be conceptualized as occurring in a single pool where the indene molecules are converted by the action of the various oxygenase and dehydrogenase enzymes depicted in Fig. 1. The steady state flux, *J*, forming and depleting any such metabolite *M* (Fig. 4A) can be determined by probing the metabolite pool with a pulse of radioactive tracer of the corresponding metabolite, *M** (in M). Assuming the system remains at steady state in the course of the experiment, the pool of intracellular *M** will change according to:

$$\frac{dM^*}{dt} = -\left(\frac{J}{M}X\right)M^* \quad (1)$$

where *X* is the biomass concentration. For constant (steady state) *M* and *J*, Eqn (1) can be integrated to give:

$$\ln\left(\frac{M^*(t)}{M^*(0)}\right) = -\left(\frac{J}{M}X\right)t \quad (2)$$

The above equation allows the determination of the unknown flux *J* from (a) the slope of the semilog plot of the normalized radioactivity counts vs. time and (b) the total metabolite pool concentration, *M*. This is a general expression for flux determination that is valid when metabolites are directly pulsed into the cells. To consider membrane transport, the culture is modeled as a two-compartment system depicting an intracellular pathway along with fluxes for the uptake (J^M_{up}) and excretion (J^M_{exc}) of metabolite *M* (Fig. 4B). Assuming that the transport of labeled (*M**) and unlabeled (*M*) metabolites are indistinguishable, the balance equations for the intracellular (M^*_{in}) and extracellular (M^*_{ex}) pools of labeled metabolite can be written as in Eqns (3) and (4), respectively.

$$\frac{dM^*_{in}}{dt} = -\left(\frac{J}{M_{in}}X\right)M^*_{in} - \left(\frac{J^M_{exc}}{M_{in}}X\right)M^*_{in} + \left(\frac{J^M_{up}}{M_{ex}}X\right)M^*_{ex} \quad (3)$$

$$\frac{dM^*_{ex}}{dt} = +\left(\frac{J^M_{exc}}{M_{in}}X\right)M^*_{in} - \left(\frac{J^M_{up}}{M_{ex}}X\right)M^*_{ex} \quad (4)$$

Adding the above equations yields a relation for the flux *J* in terms of the concentrations of the total labeled metabolite

M^*_{tot} (= M^*_{ex} + M^*_{in}), in terms of the intracellular labeled, and intracellular unlabeled metabolite pools:

$$\frac{dM^*_{tot}}{dt} = -\left(\frac{J}{M_{in}}X\right)M^*_{in} \quad (5)$$

If one further assumes that rapid equilibrium across the cell membrane is reached and that there is no distinction between the partitioning of labeled and unlabeled metabolites across the membrane (i.e. the same partition coefficient λ), the following linear relationships can be written between the intracellular and total metabolite concentrations:

$$M^*_{in} = \lambda M^*_{tot} \quad (6)$$

$$M_{in} = \lambda M_{tot} \quad (7)$$

Under these conditions, Eqn (5) can be simplified to:

$$\frac{dM^*_{tot}}{dt} = -\left(\frac{J}{M_{tot}}X\right)M^*_{tot} \quad (8)$$

Assuming constant J and M_{tot} (steady state), integration of Eqn (8) yields the following relationship for the metabolite flux in terms of the transient total labeled metabolite counts:

$$\ln\left(\frac{M^*_{tot}(t)}{M^*_{tot}(0)}\right) = -\left(\frac{J}{M_{tot}}X\right)t \quad (9)$$

The above equation suggests that the flux can be determined from the slope of a semilog plot for the fraction of the total remaining labeled metabolite in the culture vs. time. Additionally, the measurements of the biomass and total metabolite concentrations, X and M_{tot}, are required. The linearity of the semilog plot provides confirmation of the assumptions made in the derivation of Eqn (9).

This approach was applied to the investigation of the indene bioconversion network by probing the pools of *cis*-(1*S*,2*R*)-indandiol, *cis*-(1*R*,2*S*)-indandiol, and *trans*-(1*R*,2*R*)-indandiol with the corresponding radioactive compounds to determine the dehydrogenase fluxes depleting these pools. Similarly, probing with radiolabeled indene and indan oxide yielded estimates of the oxygenase and epoxide hydrolysis fluxes, respectively.

RESULTS

Metabolite concentrations remain constant during labeling

To verify that the introduction of radiolabeled probe did not significantly alter cell physiology in the course of the labeling experiment, the intracellular indene metabolite concentrations were measured for the duration of the assaying procedure. All concentrations were relatively constant for the first 50 min, indicating that steady state conditions were maintained and that the assaying procedure did not materially alter the metabolic state of the cells. The steady state intracellular concentrations were as follows (± 10 mg·L^{-1}): *trans*-indandiol, 120 mg·L^{-1}; *cis*-indandiol, 165 mg·L^{-1}; indan oxide, 25 mg·L^{-1}; 1-keto-2-hydroxy-indan, 175 mg·L^{-1}. No intracellular indene was detected. This could be due to the rapid intracellular conversion of indene or possibly the removal of indene from the cell membrane during the multilayer centrifugation.

Cell density and total metabolite concentrations were also measured. No growth was observed for the first 30 min of the assaying procedure. The total metabolite concentration profiles are shown in Fig. 5. The *trans*-indandiol, *cis*-indandiol, 1-keto-2-hydroxy-indan, and indan oxide concentrations (Fig. 5A) were constant for the first 60 min of the procedure. In contrast to these downstream metabolites, the (mainly extracellular) indene concentration changed significantly and was depleted after 60 min (Fig. 5B). Approximately 3 mg·L^{-1} of the initial indene concentration of 15 mg·L^{-1} was derived from the [^{14}C]indene pulse. As no additional indene was added to maintain this concentration, this residual amount was rapidly depleted from the medium.

Rapid equilibrium of added [^{14}C]diols

The partition coefficient λ, as defined in Eqns (6) and (7), was determined by adding [^{14}C]diols to the culture and measuring the intracellular and total concentrations of labeled and unlabeled diol. This coefficient was found to be constant over the entire 120 min of the assay procedure, with the first sample taken approximately 30 s after addition of the radiolabeled pulse, and was 0.78 ± 0.15 for unlabeled diols and 0.77 ± 0.11 for labeled diols. This provides support for the assumption of equal partitioning of labeled and unlabeled metabolites and rapid equilibrium of the labeled metabolite across the cell membrane.

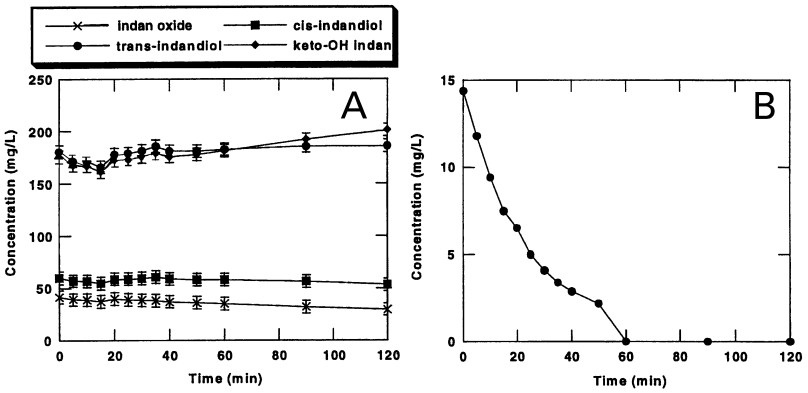

Fig. 5. Transient unlabeled total concentrations during the shake flask experiment. (A) Unlabeled *trans*-indandiol, *cis*-indandiol, 1-keto-2-hydroxy-indan, and indan oxide traces. Error bars represent the ± 6 mg·L^{-1} error resulting from the HPLC quantification. The error bars for *cis*-indandiol were omitted for clarity. (B) Unlabeled indene trace.

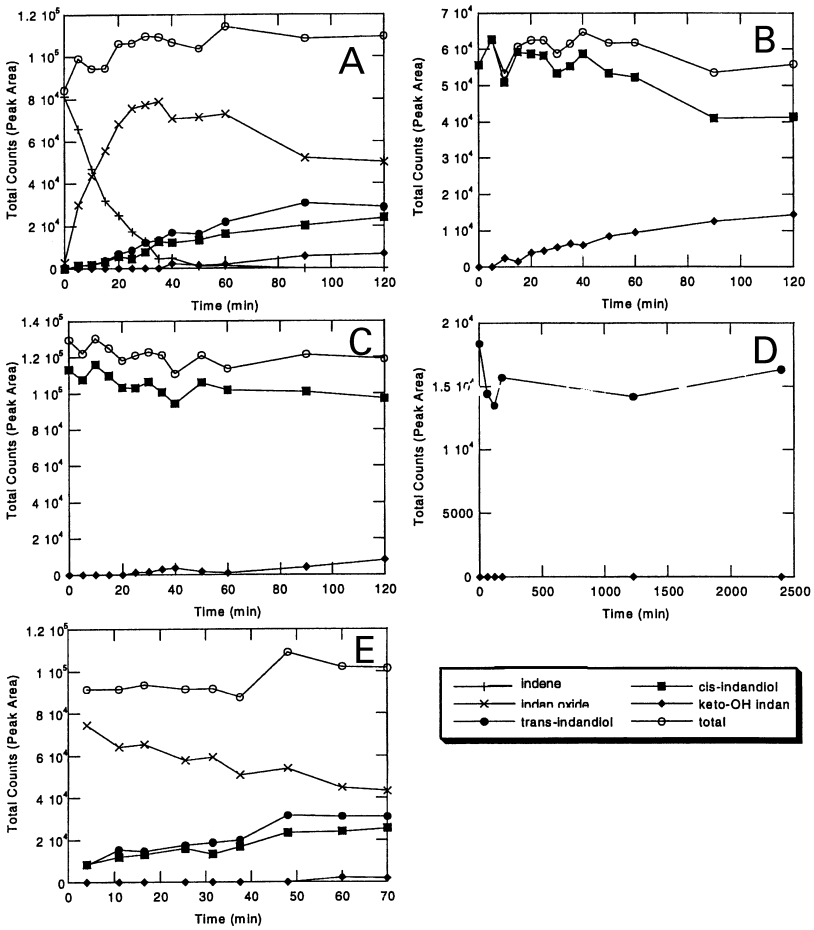

Fig. 6. Transient radiolabeled data for a dilution rate of 0.065 h^{-1} and 170 p.p.m. indene air feed concentration following a pulse of: (A) [^{14}C]indene, (B) [^{14}C]*cis*-(1*S*,2*R*)-indandiol, (C) [^{14}C]*cis*-(1*R*,2*S*)-indandiol, and (D) [^{14}C]*trans*-(1*R*,2*R*)-indandiol; and (E) [^{14}C]indan oxide transients for a dilution rate of 0.1 h^{-1} and 170 p.p.m. indene air feed concentration. The total metabolite counts for (A), (C) (D), and (E) were calculated by adding the counts of all of the metabolites present. Some *trans*-(1*R*,2*R*)-indandiol impurity was present in the *cis*-indandiol stocks for (B) and (C) accounting for the separation of *cis*-indandiol and total counts in the early time points.

^{14}C transients

Figure 6 shows the transient profiles of the total counts of indene and five indene metabolites following the introduction of various labeled compounds. These assays probed the physiology of chemostat cultures at steady state conditions obtained for dilution rates of 0.065 h^{-1} and 0.10 h^{-1} and an indene air feed concentration of 170 p.p.m. These transients are typical of other steady state conditions similarly investigated. The [^{14}C]indene label was rapidly converted to indan oxide, *trans*-indandiol, and *cis*-indandiol (Fig. 6A). The sum of all of the counts was constant for the duration of the assay procedure indicating that all major products of the indene bioconversion were detected by HPLC.

Figure 6B shows the transients following the introduction of [^{14}C]*cis*-(1*S*,2*R*)-indandiol for probing the corresponding dehydrogenase activity. Accumulation of 1-keto-2-hydroxy-indan was detected 5 min after introduction of the probe. Conversion of the [^{14}C]*cis*-(1*R*,2*S*)-indandiol tracer to 1-keto-2-hydroxy-indan was not detected until 50 min into the experiment, and only about 6% of the tracer was depleted (Fig. 6C). No conversion of [^{14}C]*trans*-(1*R*,2*R*)-indandiol was observed after 3 days of incubation with the culture (Fig. 6D). To account for any possible transport limitations through the cell membrane, the same [^{14}C]diol conversions were carried out with KY1 cell lysates (data not shown). Similar results were obtained in that *cis*-indandiol was slowly converted to 1-keto-2-hydroxy-indan, while *trans*-indandiol was not. We conclude from these results that there was no significant *trans*-(1*R*,2*R*)-indandiol dehydrogenase activity present in the KY1 strain.

Figure 6E shows the dynamics of [^{14}C](1*S*,2*R*)-indan oxide conversion by cells obtained from a steady state chemostat at 0.10 h^{-1} dilution rate. The epoxide underwent hydrolysis to form the 2*R* enantiomers of the *trans*- and *cis*-indandiol in a 4 : 3 molar ratio. The accumulation of these diols closely resembled that of the diol accumulation seen with the [^{14}C]indene tracer.

Flux determination

Total metabolite counts were plotted as suggested by Eqn (9) for the first 30 min following the introduction of the radioactive probes. Semilog plots of the normalized radioactive counts of three metabolites are shown in Fig. 7 along with the corresponding results of linear regression. Good linear fits are observed for all metabolites. Using the initial indene concentration (6.4 $mg \cdot L^{-1}$) and steady state biomass concentration in the chemostat (3.7 g dry cell weight per L), the indene uptake rate was estimated at 54 ± 5 $\mu mol \cdot h^{-1} \cdot g^{-1}$ dry cell weight.

The fluxes of two other reaction steps depicted in the KY1 network (Fig. 1) were similarly determined and are summarized in Table 1. No significant difference was observed between the slopes of the semilog plots of indan oxide depletion by cells (Fig. 7C) and cell-free supernatant (Fig. 7D), or between active and inactive cell lysates (data not shown). This evidence suggests that KY1 does not

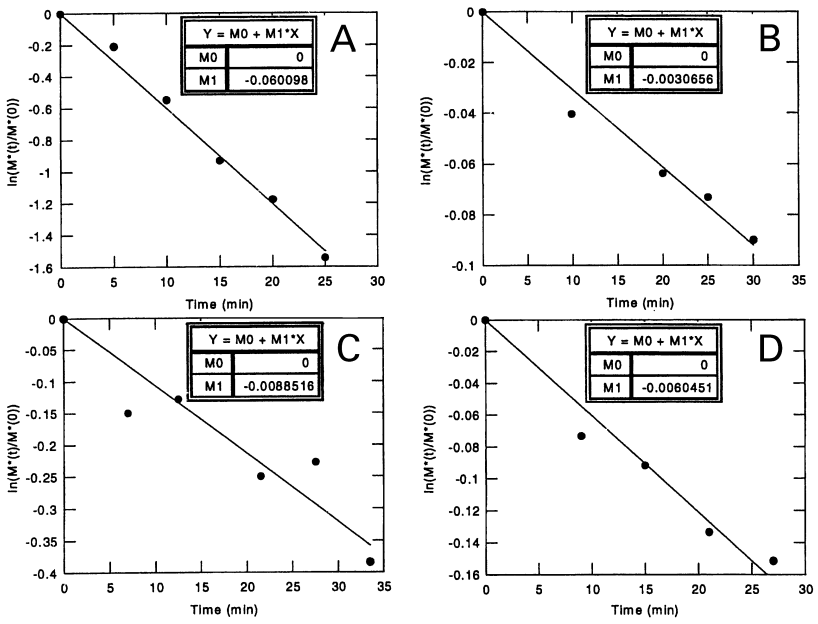

Fig. 7. Semilog plots for flux determination. (A) Indene uptake flux determination from indene depletion data after [^{14}C]indene pulse. (B) *cis*-(1*S*,2*R*)-indandiol dehydrogenase flux determination from 1-keto-2-hydroxy-indan accumulation data after [^{14}C]*cis*-(1*S*,2*R*)-indandiol pulse. *cis*-(1*S*,2*R*)-Indandiol depletion data was not used for flux determination because the decrease in [^{14}C]*cis*-(1*S*,2*R*)-indandiol was within the uncertainty of the flow scintillation measurement, shown in Fig. 6B. (C) Indan oxide hydrolysis rate determination from indan oxide depletion data after [^{14}C]indan oxide pulse in culture. (D) Indan oxide hydrolysis rate determination from indan oxide depletion data after [^{14}C]indan oxide pulse in supernatant.

contain epoxide hydrolase activity catalyzing the enzymatic hydrolysis of indan oxide. Hence, the rate constant reported in Table 1 can be used to describe the nonenzymatic hydrolysis rate for any steady state. This rate is within the uncertainty of the value independently determined using metabolite excretion and uptake rates with the direct measurement of the *cis*-(1*S*,2*R*)-indandiol dehydrogenase flux within the context of flux analysis of the indene bioconversion network (55 ± 3 μmol per h per g dry cell weight).

Flux confirmation by metabolite balancing

The indene uptake fluxes determined using ^{14}C-tracers were validated independently with fluxes derived from metabolite balances applied to extracellular chemostat metabolite measurements. To this end, the indene uptake rate was determined by two additional methods: (a) from the difference between the indene concentrations at the feed and exit lines of the reactor, and (b) by summing the residual concentrations of all indene metabolites in the chemostat (D. E. Stafford, K. S. Yamaguchi, P. A. Lessard, S. K. Rijhwani, A. J. Sinskey & G. Stephanopoulos, unpublished results). These rates are summarized in Table 2 for the two steady states obtained with a dilution rate of 0.065 h^{-1} and two different indene feed rates. Their agreement provides further support for the tracer method for determining fluxes.

Flux confirmation using a first-order kinetic model

For the KY1 pathway (Fig. 1), steady state mass balances can be written for each metabolite pool, as shown in Table 3. The fluxes (J_i) in the KY1 indene bioconversion network can then be calculated using these balances, the metabolite production rates (r_i) determined from chemostat steady state concentration measurements, and the *cis*-(1*S*,2*R*)-indandiol dehydrogenase flux (J_{RDH}) determined from the ^{14}C-tracer experiment. These flux distributions and metabolite pool concentrations for two different steady states are shown in Fig. 8. The same steady state fluxes and concentrations can be used to fit a first-order kinetic model describing the conversion of a [^{14}C]indene pulse in steady state cells. Predictions of this model were compared to the experimental transient ^{14}C-metabolite profiles obtained following [^{14}C]indene addition to steady state culture samples taken from the chemostat as a method to verify the flux estimates.

For constant $[M_{tot}]$ during the ^{14}C assaying experiment, where $[M_{tot}] << K_m$ for the respective enzymatic activity assuming Michaelis–Menten kinetics, Eqn (8) can be expressed as a first-order rate equation with respect to the labeled metabolite concentration:

$$\frac{d[M^*_{tot}]}{dt} = -k_i[M^*_{tot}] \quad (10)$$

where

$$k_i = \frac{J_i}{[M_{tot}]}X \quad (11)$$

Table 1. Pathway fluxes determined using ^{14}C tracers. DCW, dry cell weight.

Reaction Step	Rate constant (h^{-1})	Metabolite concentration ($mg \cdot L^{-1}$)	Biomass concentration ($g \cdot L^{-1}$)	Flux ($\mu mol \cdot h^{-1} \cdot g\ DCW^{-1}$)
Indene Uptake	0.060 ± 0.006	6.4	3.7	54 ± 5
cis-(1*S*,2*R*)-indandiol Dehydrogenase	0.0031 ± 0.0002	54	3.7	18 ± 2
Indan oxide Hydrolysis	0.009 ± 0.001	53	3.7	59 ± 7

Table 2. Comparison of indene uptake rates determined using three different methods. DCW, dry cell weight.

	Indene uptake rate (μmol·h^{-1}·g DCW^{-1})		
Steady State	^{14}C Transients	Chemostat balance	Cellular balance
100 p.p.m.	24 ± 3	28 ± 5	28 ± 2
170 p.p.m.	54 ± 5	63 ± 10	63 ± 3

As shown in Fig. 5, the total metabolite concentration for all metabolites except indene were constant for the first 60 min of the assay procedure.

With the expression of Eqn (11), the reaction rate constants k_i can be determined from the flux estimates calculated independently through material balancing and the corresponding metabolite pool concentrations. The dynamics of [^{14}C]indene oxidation through the KY1 indene bioconversion network can then be predicted using these reaction rate constants from the integration of the dynamic metabolite balance Eqns (12–17):

$$\frac{d\left[I^*_{tot}\right]}{dt} = -(k_{MO} + k_{DO})\left[I^*_{tot}\right] \quad (12)$$

$$\frac{d\left[IO^*_{tot}\right]}{dt} = k_{MO}\left[I^*_{tot}\right] - (k_{C2R} + k_T)\left[IO^*_{tot}\right] \quad (13)$$

$$\frac{d\left[T^*_{tot}\right]}{dt} = k_T\left[IO^*_{tot}\right] \quad (14)$$

$$\frac{d\left[C2R^*_{tot}\right]}{dt} = k_{C2R}\left[IO^*_{tot}\right] - k_{RDH}\left[C2R^*_{tot}\right] \quad (15)$$

$$\frac{d\left[C2S^*_{tot}\right]}{dt} = k_{DO}\left[I^*_{tot}\right] - k_{SDH}\left[C2S^*_{tot}\right] \quad (16)$$

$$\frac{d\left[K^*_{tot}\right]}{dt} = k_{RDH}\left[C2R^*_{tot}\right] + k_{SDH}\left[C2S^*_{tot}\right] \quad (17)$$

It is noted that as the indene concentration, $[I_{tot}]$, is not constant through the course of the assaying procedure (Fig. 5B), this first-order kinetic model is only satisfied for

Table 3. Steady state metabolite balances for the KY1 indene bioconversion network.

Metabolite pool	Balance equation
Indene	$r_{IND} - J_{MO} - J_{DO} = 0$
Indan oxide	$J_{MO} - J_T - J_{C2R} - r_{IO} = 0$
trans-(1*R*,2*R*)-Indandiol	$J_T - r_T = 0$
cis-(1*S*,2*R*)-Indandiol	$J_{C2R} - J_{RDH} - r_{C2R} = 0$
cis-(1*R*,2*S*)-Indandiol	$J_{DO} - J_{SDH} - r_{C2S} = 0$
1-Keto-2-hydroxy-indan	$J_{RDH} + J_{SDH} - r_K = 0$

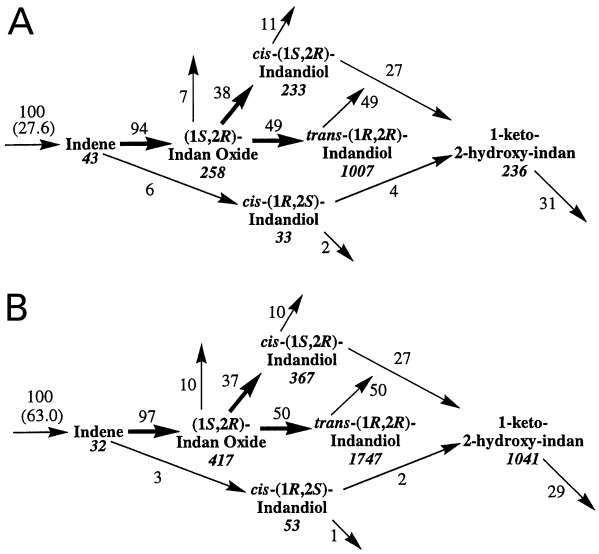

Fig. 8. Steady state intracellular flux distribution and metabolite pool concentrations (in μM and italicized under the corresponding pool) for two KY1 culture conditions determined by metabolite balancing: (A) dilution rate of 0.065 h^{-1} and 100 p.p.m. indene air feed concentration and (B) dilution rate of 0.065 h^{-1} and 170 p.p.m. indene air feed concentration. The fluxes were normalized by the indene uptake rate (in parentheses: μmol·h^{-1}·g DCW^{-1}).

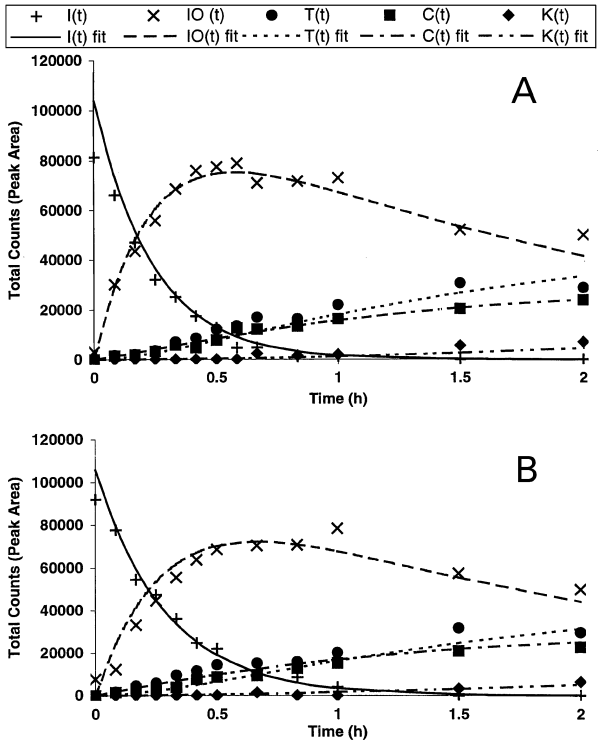

Fig. 9. Kinetic model fit to [^{14}C]indene tracer data for steady states at a dilution rate of 0.065 h^{-1} and (A) 100 p.p.m. indene air feed concentration and (B) 170 p.p.m. indene air feed concentration. $I(t)$, $IO(t)$, $T(t)$, $C(t)$, and $K(t)$ are the data for ^{14}C-labeled indene, indan oxide, *trans*-indandiol, *cis*-indandiol, and 1-keto-2-hydroxy-indan, respectively.

relatively low concentrations of the indene substrate (for other symbols, please see Fig. 1). The predictions of this first order model were compared to the [^{14}C]indene pulse experimental data (Fig. 9). The agreement between the experimental data and the predicted profiles validates the estimated flux results and demonstrates further utility of the radiolabeled tracers as tools for flux analysis.

DISCUSSION

This work has shown that radiolabeled tracers are a valuable aid in the characterization of complex bioconversion networks. ^{14}C-Labeled tracers are particularly useful for systems in which there is no alteration of the carbon skeleton. Fluxes can be determined directly from transient ^{14}C-tracer experiments because of the high sensitivity in quantifying labeled compounds by HPLC and liquid flow scintillation counting. The ^{14}C-tracer experiments are short-term, simple to carry out and require only linear regression analysis of the data. For reliable flux estimation using this method, key assumptions about the system being studied must be verified: (a) the organism must be able to take up the radiolabeled molecule; (b) the radiolabeled pulse does not perturb the steady state of the culture; (c) the culture remains at a steady state for the duration of the experiment; (d) if a metabolite concentration changes with time, its concentration must be significantly below the K_m value of the enzyme being studied; and (e) the reaction under analysis is irreversible.

The first assumption should obviously be true for the precursor substrate with any organism, but must be verified for intermediate pathway metabolites. The second assumption is generally met when the material added by the pulse is only a small fraction of the unlabeled metabolite pool. Assumption (c) depends on the kinetics of the pathway enzymes and should be verified by measuring the intracellular concentrations during the experiment. The duration of the experiment may need to be shortened if there are significant changes in concentration. Otherwise, assumption (d) may be applied if there are only trace amounts of the desired metabolite present. If assumption (e) is not valid, the analysis of tracer data becomes considerably more complex. However, the irreversibility of a given reaction is verifiable both through the tracer experiments described here and using redundant measurements and metabolite balancing in the context of metabolic flux analysis.

The additional assumption of rapid equilibrium of the radiolabeled metabolite across the cell membrane allows for simplification of the experimental protocol as it eliminates the need for intracellular residual metabolite measurements. This assumption depends on the cell's transport mechanisms for the metabolites. If an active transport mechanism is present, rapid equilibrium should be a reasonable assumption. If only passive transport occurs, the transport kinetics must be significantly faster than the bioconversion enzyme kinetics. For bioconversion of aromatic substrates, the transport is frequently passive and fairly rapid through the cell membrane (due to its hydrophobic nature) although active transport has also been shown to occur [48].

Radiolabeled tracers can also be used to study the effects of culture conditions on key pathway enzymes. For the KY1 indene bioconversion, radiolabeled tracers permitted the quantification of the inhibitory effect that *trans*-(1*R*,2*R*)-indandiol and 1-keto-2-hydroxy-indan have on the indene monooxygenase activity (unpublished data). Results showed that both metabolites significantly inhibit the monooxygenase enzyme at concentrations as low as 1.0 g·L^{-1}.

The pathway fluxes yielded useful information about the bioconversion pathway structure: First, KY1 is phenotypically different from its parent, I24, and the [^{14}C]indene probing experiments demonstrated that KY1 lacks the dioxygenase enzyme activity present in I24 that is responsible for conversion of indene to *cis*-(1*S*,2*R*)-indandiol and 1-indenol (D. E. Stafford, K. S. Yamaguchi, P. A. Lessard, S. K. Rijhwani, A. J. Sinskey & G. Stephanopoulos, unpublished results). Second, the primary pathway of indene oxidation in KY1 is through the monooxygenase enzyme that is responsible for converting over 94% of the indene taken up to (1*S*,2*R*)-indan oxide (Fig. 8). Indan oxide is hydrolyzed to both *trans* and *cis* diastereomers of (2*R*)-indandiol, both of which are suitable precursors for the synthesis of (−)-CAI. However, the *cis*-(1*S*,2*R*)-indandiol is further degraded to racemic 1-keto-2-hydroxy-indan, wasting approximately 25% of the total indene consumed. Third, the KY1 bioconversion network lacks *trans*-(1*R*,2*R*)-indandiol dehydrogenase and epoxide hydrolase activities. Integrating this additional knowledge about the KY1 bioconversion network allows the identification of promising candidate targets for genetic modification to increase the (2*R*)-indandiol product yield. One such target is the introduction of an epoxide hydrolase activity alone or in combination with a knockout of the dioxygenase and *cis*-(1*S*,2*R*)-indandiol dehydrogenase. This strategy would direct the hydrolysis reaction towards the formation of *trans*-indandiol and thus minimize (or eliminate) the formation of the 1-keto-2-hydroxy-indan byproduct. Indeed, the transformation of KY1 with the *limA* gene encoding for an epoxide hydrolase from *R. erythropolis* DCL14 increased the selectivity of indene oxidation toward *trans*-(1*R*,2*R*)-indandiol (D. E. Stafford, K. S. Yamaguchi, P. A. Lessard, S. K. Rijhwani, A. J. Sinskey & G. Stephanopoulos, unpublished results).

We note that the *trans*-(1*R*,2*R*)-indandiol and 1-keto-2-hydroxy-indan are also inhibitory to the monooxygenase enzyme. Thus, the monooxygenase is a candidate for overexpression and directed evolution to remove product inhibition effects. The dioxygenase pathway plays only a minor role in indene bioconversion.

ACKNOWLEDGEMENTS

This work was supported by a grant from Merck Research Laboratories. K. Y. and D. E. S. were supported in part by National Institute of Health (NIH) Biotechnology Training Grant # 2T32 GM08334-10 and by the Engineering Research Program of BES, Department of Energy Grant no. DE-FG02–94ER-14487. We also acknowledge the supply by Merck of the ^{14}C materials (synthesized by M. Braun).

REFERENCES

1. Aiba, S. & Matsuoka, M. (1979) Identification of metabolic model: citrate production from glucose by *Candida lipolytica*. *Biotechnol. Bioeng.* **21**, 1373–1386.
2. Stephanopoulos, G., Aristidou, A.A. & Nielsen, J. (1998). *Metabolic Engineering*. Academic Press, San Diego.

3. Stephanopoulos, G. (1999) Metabolic fluxes and metabolic engineering. *Metabolic Eng.* **1**, 1–11.
4. Vallino, J.J. & Stephanopoulos, G. (1993) Metabolic flux distributions in *Corynebacterium glutamicum* during growth and lysine overproduction. *Biotechnol. Bioeng.* **41**, 633–646.
5. Vallino, J.J. & Stephanopoulos, G. (1994) Carbon flux distributions at the pyruvate branch point in *Corynebacterium glutamicum* during lysine overproduction. *Biotechnol. Prog.* **10**, 320–326.
6. Holms, H. (1996) Flux analysis and control of the central metabolic pathways in *Escherichia coli*. *FEMS Microbiol. Rev.* **19**, 85–116.
7. Farmer, W.R. & Liao, J.C. (1997) Reduction of aerobic acetate production by *Escherichia coli*. *Appl. Environ. Microbiol.* **63**, 3205–3210.
8. Delgado, J. & Liao, J.C. (1997) Inverse flux analysis for reduction of acetate excretion in *Escherichia coli*. *Biotechnol. Prog.* **13**, 361–367.
9. Aristidou, A.A., San, K.Y. & Bennett, G.N. (1999) Metabolic flux analysis of *Escherichia coli* expressing the *Bacillus subtilis* acetolactate synthase in batch and continuous cultures. *Biotechnol. Bioeng.* **63**, 737–749.
10. Hua, Q., Yang, C. & Shimizu, K. (1999) Metabolic flux analysis for efficient pyruvate fermentation using vitamin-auxotrophic yeast of *Torulopsis glabrata*. *J. Biosci. Bioeng.* **87**, 206–213.
11. Jin, S., Ye, K.M. & Shimizu, K. (1997) Metabolic flux distributions in recombinant *Saccharomyces cerevisiae* during foreign protein production. *J. Biotechnol.* **54**, 161–174.
12. Follstad, B.D., Balcarcel, R.R., Stephanopoulos, G. & Wang, D.I.C. (1999) Metabolic flux analysis of hybridoma continuous culture steady state multiplicity. *Biotechnol. Bioeng.* **63**, 675–683.
13. Paredes, C., Sanfeliu, A., Cardenas, F., Cairo, J.J. & Godia, F. (1998) Estimation of the intracellular fluxes for a hybridoma cell line by material balances. *Enzyme Microb. Technol.* **23**, 187–198.
14. Bonarius, H.P.J., Hatzimanikatis, V., Meesters, K.P.H., deGooijer, C.D., Schmid, G. & Tramper, J. (1996) Metabolic flux analysis of hybridoma cells in different culture media using mass balances. *Biotechnol. Bioeng.* **50**, 299–318.
15. Lee, K., Berthiaume, F., Stephanopoulos, G.N. & Yarmush, M.L. (1999) Metabolic flux analysis: a powerful tool for monitoring tissue function. *Tissue Eng.* **5**, 347–368.
16. Bonarius, H.P.J., Schmid, G. & Tramper, J. (1997) Flux analysis of underdetermined metabolic networks: the quest for the missing constraints. *Trends Biotechnol.* **15**, 308–314.
17. Park, S.M., Klapa, M.I., Sinskey, A.J. & Stephanopoulos, G. (1999) Metabolite and isotopomer balancing in the analysis of metabolic cycles: II. Applications. *Biotechnol. Bioeng.* **62**, 392–401.
18. Marx, A., de Graaf, A.A., Wiechert, W., Eggeling, L. & Sahm, H. (1996) Determination of the fluxes in the central metabolism of *Corynebacterium glutamicum* by nuclear magnetic resonance spectroscopy combined with metabolite balancing. *Biotechnol. Bioeng.* **49**, 111–129.
19. Inbar, L. & Lapidot, A. (1987) C-13-Nmr, H-1-Nmr and gas-chromatography mass-spectrometry studies of the biosynthesis of C-13-enriched L-lysine by *Brevibacterium flavum*. *Eur. J. Biochem.* **162**, 621–633.
20. Walsh, K. & Koshland, D.E. (1984) Determination of flux through the branch point of 2 metabolic cycles – the tricarboxylic-acid cycle and the glyoxylate shunt. *J. Biol. Chem.* **259**, 9646–9654.
21. Zupke, C. & Stephanopoulos, G. (1994) Modeling of isotope distributions and intracellular fluxes in metabolic networks using atom mapping matrices. *Biotechnol. Prog.* **10**, 489–498.
22. Zupke, C. & Stephanopoulos, G. (1995) Intracellular flux analysis in hybridomas using mass balances and *in vitro* C-13 NMR. *Biotechnol. Bioeng.* **45**, 292–303.
23. Sharfstein, S.T., Tucker, S.N., Mancuso, A., Blanch, H.W. & Clark, D.S. (1994) Quantitative *in vivo* nuclear-magnetic-resonance studies of hybridoma metabolism. *Biotechnol. Bioeng.* **43**, 1059–1074.
24. Portais, J.C., Schuster, R., Merle, M. & Canioni, P. (1993) Metabolic flux determination in C6 Glioma-cells using C-13 distribution upon [1-C-13]glucose incubation. *Eur. J. Biochem.* **217**, 457–468.
25. Jucker, B.M., Lee, J.Y. & Shulman, R.G. (1998) *In vivo* C-13 NMR measurements of hepatocellular tricarboxylic acid cycle flux. *J. Biol. Chem.* **273**, 12187–12194.
26. Fernandez, C.A. & Rosiers, C.D. (1995) Modeling of liver citric-acid cycle and gluconeogenesis based on C-13 mass isotopomer distribution analysis of intermediates. *J. Biol. Chem.* **270**, 10037–10042.
27. Malloy, C.R., Sherry, A.D. & Jeffrey, F.M.H. (1988) Evaluation of carbon flux and substrate selection through alternate pathways involving the citric-acid cycle of the heart by C-13 Nmr-spectroscopy. *J. Biol. Chem.* **263**, 6964–6971.
28. Malloy, C.R., Sherry, A.D. & Jeffrey, F.M.H. (1990) Analysis of tricarboxylic-acid cycle of the heart using C-13 isotope isomers. *Am. J. Physiol.* **259**, H987–H995.
29. Chance, E.M., Seeholzer, S.H., Kobayashi, K. & Williamson, J.R. (1983) Mathematical-analysis of isotope labeling in the citric-acid cycle with applications to C-13 Nmr-studies in perfused rat hearts. *J. Biol. Chem.* **258**, 3785–3794.
30. Messana, I., Misiti, F., el-Sherbini, S., Giardina, B. & Castagnola, M. (1999) Quantitative determination of the main glucose metabolic fluxes in human erythrocytes by C-13- and H-1-MR spectroscopy. *J. Biochem. Biophys. Meth* **39**, 63–84.
31. Berthon, H.A., Bubb, W.A. & Kuchel, P.W. (1993) C-13 NMR isotopomer and computer-simulation studies of the nonoxidative pentose-phosphate pathway of human erythrocytes. *Biochem. J.* **296**, 379–387.
32. Schmidt, K., Marx, A., de Graaf, A.A., Wiechert, W., Sahm, H., Nielsen, J. & Villadsen, J. (1998) C-13 tracer experiments and metabolite balancing for metabolic flux analysis: comparing two approaches. *Biotechnol. Bioeng.* **58**, 254–257.
33. Christensen, B. & Nielsen, J. (2000) Metabolic network analysis of *Penicillium chrysogenum* using C-13-labeled glucose. *Biotech. Bioeng.* **68**, 652–659.
34. Allsop, J.R. & Wolfe. R.R. (1979) The reliability of rates of glucose appearance *in vivo* calculated from single tracer injections. *Can. J. Physiol. Pharmacol.* **57**, 1267–1274.
35. Jacquez, J.A. (1992) Theory of production rate calculations in steady and non-steady states and its application to glucose metabolism. *Am. J. Physiol.* **262**, E779–E790.
36. Hovorka, R., Eckland, D.J.A., Halliday, D., Lettis, S., Robinson, C.E., Bannister, P., Young, M.A. & Bye, A. (1997) Constant infusion and bolus injection of stable-label tracer give reproducible and comparable fasting HGO. *Am. J. Physiol. Endocrinol. Metab.* **36**, E192–E201.
37. Buckland, B.C., Drew, S.W., Connors, N.C., Chartrain, M,M, Lee, C., Salmon, P.M., Gbewonyo, K., Zhou, W., Gailliot, P., Singhvi, R. et al. (1999) Microbial conversion of indene to indandiol: a key intermediate in the synthesis of CRIXIVAN. *Metabolic Eng.* **1**, 63–74.
38. Chartrain, M., Jackey, B., Taylor, C., Sandford, V., Gbewonyo, K., Lister, L., DiMichelle, L., Hirsch, C., Heimbuch, B., Maxwell, C. *et al*. (1998) Bioconversion of indene to *cis* (1*S*,2*R*) indandiol and *trans* (1*R*,2*R*) indandiol by *Rhodococcus* species. *J. Ferm. Bioeng.* **86**, 550–558.
39. Treadway, S.L., Yanagimachi, K.S., Lankenau, E., Lessard, P.A., Stephanopoulos, G. & Sinskey, A.J. (1999) Isolation and characterization of indene bioconversion genes from *Rhodococcus* strain I24. *Appl. Micro. Biotech.* **51**, 786–793.
40. Khalaf, A.A., Abdel-Wahab, A.A., El-Khawaga, A.M. & El-Zohry, M.F. (1984) Modern Friedel–Crafts chemistry XIII. Intra- and intermolecular cyclization of some carbonyl derivates under Friedel–Crafts conditions. *Bull. Chem. Soc. France* **II**, 285–291.

41. Stang, P.J. & Fisk, T.E. (1979) Synthesis of 1-(ethynyl)-vinyl trifluoromethanesulfonates. *Synthesis*, 438–440.
42. Kotsuki, H., Datta, P.K., Hayakawa, H. & Suenaga, H. (1995) An efficient procedure for palladium-catalyzed reduction of aryl/enol triflates. *Synthesis*, 1348–1350
43. Larrow, J.F., Roberts, E., Verhoeven, T.R., Ryan, K.M., Senanayake, C.H., Reider, P.J. & Jacobsen, E.N. (1998) (1*S*,2*R*)-1-aminoindan-2-ol. *Organic Synthesis* **76**, 46–56.
44. Guerlava, P., Izac, V. & Tholozan, J.-L. (1997) Comparison of different methods of cell lysis and protein measurements in *Clostridium perfringens*: application to the cell volume determination. *Curr. Microbiol.* **36**, 131–135.
45. Clement, Y., Escoffier, B., Trombe, M.C. & Lanéelle, G. (1984) Is glutamate excreted by its uptake system in *Corynebacterium glutamicum*? A working hypothesis. *J. Gen. Microbiol.* **130**, 2589–2594.
46. Klingenberg, M. & Pfaff, E. (1967) Means of terminating reactions. In *Methods in Enzymology*, **Vol. X** (Estabrook, R.W. & Pullman, M.R., eds), pp. 680–684. Academic Press, Inc., New York.
47. Wolfe, R.R. (1992) *Radioactive and Stable Isotope Tracers in Biomedicine: Principles and Practice of Kinetic Analysis*. Wiley-Liss, Inc., New York.
48. Whitman, B.E., Lueking, D.R. & Mihelcic, J.R. (1998) Naphthalene uptake by a *Pseudomonas fluorescens* isolate. *Can. J. Microbiol.* **44**, 1086–1093.